Simple determinant representation for rogue waves of the nonlinear Schrödinger equation

Liming Ling[1] and Li-Chen Zhao[2,*]
[1]*Department of Mathematics, South China University of Technology, Guangzhou 510640, China*
[2]*Department of Physics, Northwest University, Xi'an 710069, China*
(Received 19 June 2013; revised manuscript received 13 August 2013; published 2 October 2013)

We present a simple representation for arbitrary-order rogue wave solution and a study on the trajectories of them explicitly. We find that the trajectories of two valleys on whole temporal-spatial distribution all look "X" -shaped for rogue waves. Additionally, we present different types of high-order rogue wave structures, which could be helpful towards realizing the complex dynamics of rogue waves.

DOI: 10.1103/PhysRevE.88.043201 PACS number(s): 46.40.−f, 03.75.Kk, 03.75.Lm, 67.85.Hj

I. INTRODUCTION

Rogue wave (RW) is localized both in space and time and depicts a unique event which seems to appear from nowhere and disappear without a trace [1–5]. Many studies indicate that nonlinear theories can be used to explain the dramatic phenomenon [6–8]. Among nonlinear theories, the most fundamental is based on the nonlinear Schrödinger equation (NLSE) [9]

$$i\frac{\partial u(x,t)}{\partial t}+\frac{\partial^2 u(x,t)}{\partial x^2}+2|u(x,t)|^2u(x,t)=0, \qquad (1)$$

which can be used to describe the dynamics of localized waves in many physical systems, such as nonlinear fiber [6], Bose-Einstein condensate [10], plasma system [8], and even water wave tank [7]. Particularly, the wave function describes the evolution of the electromagnetic field propagating in nonlinear optics where the z component takes the place of the t component [11]. It can describe one-dimensional ocean waves—the focusing (defocusing) NLSE when dealing with deep (shallow) narrow-banded water waves [12,13]. The wave function can be the order parameter describing Bose-Einstein condensates (the NLSE is called the Gross-Pitaevskii equation in this field), for which the defocusing NLSE (repulsive interactions between atoms) is most of the time used as the focusing case (attractive interactions between atoms) in more than one dimension leads to collapse events in the condensate [14].

The rational solution of the nonlinear equation has been used to describe the RW phenomenon [6–8]. It is now already more than 30 years since the first breather solution of the NLSE was found by Ma [15], which breathes temporally but is spatially localized. Akhmediev found a kind of solutions [16,17] qualitatively different from Ma breathers, which were called breathers by Akhmediev . The Akhmediev breathers breathe spatially but are localized in time. Simply speaking, Akhmediev breathers are exact solutions of the NLSE that start from modulation instability of a plane wave [17] (also known as a Benjamin-Feir [18–20] or Bespalov-Talanov instability) and return to a plane wave at the end of the evolution. Peregrine gave a solution localized in both space and time in 1983 [21], which can be seen as the limit of the Ma breather and the Akhmediev breather. Recently, the Peregrine rational solution (fundamental RW), the second-order RW, and solutions up to order 5 have been observed in a water wave tank [7,22–24]. Also, the rogue waves described by the Peregrine rational solution have been generated in optics [6,25] and magnetoplasma [26,27]. Thus, the validity of the simplest RW solutions has been confirmed experimentally. This also means that the simple presentation and the quality for RW solutions is crucial for further research in this area.

Darboux transformation, originating from the work of Darboux in 1882 on the Sturm-Liouville equation, is a powerful method for constructing solutions for integrable systems. The theory is presented in several monographs and review papers (see [28–30]). Various approaches have been proposed to find a Darboux transformation for a given equation, for instance, the operator factorization method [31], the gauge transformation method [30,32,33], and the loop group transformation [34]. The classical Darboux transformation can be used to derive a fundamental RW solution. However, it cannot be applied to derive high-order RW solutions since the classical Darboux transformation cannot be iterated at the same spectral parameter. To overcome this difficulty, Guo, Liu, and the first author of this paper used the limit technique to generalize the classical Darboux transformation [35,36], which can be used to yield a high-order solution. Based on this simple idea, there are a series of research papers about high-order RW solutions for other integrable systems [37,38]. It should be pointed out that based on direct recursive Darboux transformation, a numeric method and limit technique can be used to construct high-order rogue wave solutions [39–42]. Comparing with the previous method, we can give a simple representation for general high-order RW solutions. Besides Darboux' related method, there are also some other methods to derive general high-order RW solutions [43–46].

In this paper, we present a simple representation for general NLSE RW solution, and investigate the dynamics and kinetics of RWs explicitly. We find the whole trajectories for high-order RWs are similar to that of the first-order RW, whose trajectory looks like an "X." They are different around the location where the RW happens. In addition, we discuss their classification by parameters s_i. We present some different structures for general fourth-order rogue waves, such as "double column" structure and "claw-line" structure.

II. A SIMPLE REPRESENTATION FOR GENERAL RW SOLUTION

In this section, we derive a generalized expression for arbitrary Nth-order RW solution of Eq. (1). The Lax pair for

*zhaolichen3@163.com

NLSE (1) is [47]

$$\begin{aligned}\Psi_x &= (-i\lambda\sigma_3 + iQ)\Psi,\\ \Psi_t &= (2i\lambda^2\sigma_3 - 2i\lambda Q - i\sigma_3 Q^2 + \sigma_3 Q_x)\Psi,\end{aligned} \tag{2}$$

where

$$\sigma_3 = \begin{pmatrix}1 & 0\\ 0 & -1\end{pmatrix}, \quad Q = \begin{pmatrix}0 & \bar{u}\\ u & 0\end{pmatrix}.$$

Previously we presented some lemmas about generalized Darboux transformation.

Lemma 1 ([35,36]). Suppose we have N different solutions Φ_i for system (2) with $\lambda = \lambda_i$; then the N-fold Darboux transformation

$$T_N = I + \sum_{i=1}^{N} \frac{T_i}{\lambda - \bar{\lambda}_i} = I - XM^{-1}(\lambda - D)^{-1}X^{\dagger},$$

where

$$\begin{aligned}M &= \left(\frac{\Phi_i^{\dagger}\Phi_j}{\lambda_j - \bar{\lambda}_i}\right)_{1\leqslant i,j\leqslant N},\\ X &= [\Phi_1, \Phi_2, \ldots, \Phi_N],\\ D &= \mathrm{diag}(\bar{\lambda}_1, \bar{\lambda}_2, \ldots, \bar{\lambda}_N),\end{aligned}$$

converts system (2) into a new system

$$\begin{aligned}\Psi[N]_x &= (-i\lambda\sigma_3 + iQ[N])\Psi[N],\\ \Psi[N]_t &= (2i\lambda^2\sigma_3 - 2i\lambda Q[N] - i\sigma_3 Q[N]^2\\ &\quad + \sigma_3 Q[N]_x)\Psi[N],\end{aligned}$$

where

$$Q[N] = \begin{pmatrix}0 & \overline{u[N]}\\ u[N] & 0\end{pmatrix}, \quad u[N] = u - 2\sum_{i=1}^{N} T_i[2,1],$$

$$\sum_{i=1}^{N} T_i[2,1] = \frac{\det(M_1)}{\det(M)}, \quad M_1 = \begin{pmatrix}M & (M[1])^{\dagger}\\ M[2] & 0\end{pmatrix},$$

$$M[i] = [\Phi_1[i], \Phi_2[i], \ldots, \Phi_N[i]].$$

$\Phi_m[i]$ is the ith component of vector Φ_m, $m = 1,2,\ldots,N$, $i = 1,2$.

As we know from Ref. [35], the generalized Darboux transformation is nothing but a special limit for N-fold Darboux transformation. Based on the above lemma, we can obtain the following theorem to general high-order rogue wave solution.

Theorem 1. The general RW solution formula of a NLSE is

$$u(x,t) = \left(1 - 2\frac{\det(A_1)}{\det(A)}\right)\exp(2it), \tag{3}$$

and its density expression can be derived as

$$|u|^2 = 1 + [\ln \det(A)]_{xx}\,. \tag{4}$$

The expressions for A_1 and A are

$$A_1 = \begin{pmatrix}A & A[2]\\ A[1] & 0\end{pmatrix}, \quad A = (A_{l,j})_{1\leqslant l,j\leqslant N}, \tag{5}$$

where

$$A[1] = [\phi_0, \phi_1, \ldots, \phi_{N-1}], \quad A[2] = [\bar{\psi}_0, \bar{\psi}_1, \ldots, \bar{\psi}_{N-1}]^T.$$

The variable functions ψ_j, ϕ_j, and $A_{i,j}$ are the related Taylor expansion coefficients of the following functions:

$$\begin{aligned}\psi &= i(C_1X - C_2X^{-1}) \equiv \sum_{i=0}^{+\infty}\psi_i f^{2i},\\ \phi &= C_2X - C_1X^{-1} \equiv \sum_{i=0}^{+\infty}\phi_i f^{2i},\\ A(f,\bar{f}) &= \frac{i(\psi\bar{\psi} + \phi\bar{\phi})}{2 + f^2 + \bar{f}^2} = \sum_{l,j=1}^{+\infty,+\infty} A_{l,j} f^{2(l-1)}\bar{f}^{2(j-1)},\\ \psi_i &= \frac{1}{(2i)!}\frac{\partial^{2i}\psi}{\partial f^{2i}}\bigg|_{f=0}, \quad \phi_i = \frac{1}{(2i)!}\frac{\partial^{2i}\phi}{\partial f^{2i}}\bigg|_{f=0},\\ A_{l,j} &= \frac{1}{[2(l-1)]!\,[2(j-1)]!}\frac{\partial^{2(l+j-2)}A(f,\bar{f})}{\partial f^{2(l-1)}\partial\bar{f}^{2(j-1)}}\bigg|_{f=0},\end{aligned} \tag{6}$$

where $C_1 = \frac{\sqrt{1+f^2}-h}{h}$, $C_2 = \frac{\sqrt{1+f^2}+h}{h}$, $X = e^{h[x+2it+2itf^2+S(f)]}$, $h = f\sqrt{2+f^2}$, and $S(f) = \sum_{i=1}^{N-1} s_i f^{2i}$ (s_i is a complex constant). The symbol overbar represents the complex conjugation.

Proof: We prove this theorem based on the generalized Darboux transformation. We neglect the proof for the generalized Darboux transformation, since the details are given in Refs. [28,34–36,48].

From the seed solution for NLSE (1) $u[0] = \exp[2it]$, we have the fundamental solution for Lax pair (2):

$$\begin{aligned}\Psi_0 = \exp[-it\sigma_3]&\begin{pmatrix}1 & \sqrt{1+\lambda^2} - \lambda\\ \lambda - \sqrt{1+\lambda^2} & 1\end{pmatrix}\\ &\times \exp[-i(1+\lambda^2)^{1/2}(x - 2\lambda t)\sigma_3].\end{aligned} \tag{7}$$

Together with the generalized Darboux transformation T [35,36], we can obtain the fundamental solution matrix $\Psi = T\Psi_0$ for the general rogue wave solution u. Furthermore, the solution matrix can be expanded in the following form:

$$\Psi = E\,\exp[-i\lambda\sigma_3(x - 2\lambda t)], \quad \text{as } \lambda \to \infty^{+}.$$

Here $E = I + E_1\lambda^{-1} + E_2\lambda^{-2} + O(\lambda^{-3})$. Substituting into (2), we have

$$\begin{aligned}E_x &= -i\lambda[\sigma_3, E] + iQE,\\ E_t &= 2i\lambda^2[\sigma_3, E] + (-2i\lambda Q - \mathrm{i}\sigma_3 Q^2 + \sigma_3 Q_x)E.\end{aligned}$$

Comparing the coefficients of the above two equations, we then have

$$\begin{aligned}Q = [\sigma_3, E_1], \quad E_{1,x} &= -i[\sigma_3, E_2] + iQE_1,\\ 2i[\sigma_3, E_2] - i\sigma_3 Q^2 + \sigma_3 Q_x - 2\mathrm{i}QE_1 &= 0.\end{aligned}$$

It follows that

$$\sigma_3 Q^2 = 2iE_{1,x}^{\mathrm{diag}}.$$

To realize the above expansion form, the Taylor expansion for $\sqrt{1+\lambda^2}$ is essential:

$$\sqrt{1+\lambda^2} = \lambda + \tfrac{1}{2}\lambda^{-1} - \tfrac{1}{8}\lambda^{-3} + O(\lambda^{-5}).$$

Together with the Darboux transformation [35,36]

$$T = I + \sum_{i=1}^{N} \frac{T_i}{\lambda - \bar{\lambda}_i},$$

then the exact expression of E_1 is

$$E_1 = -\frac{ix}{2}\sigma_3 + \frac{1}{2}\begin{pmatrix} 0 & e^{-2it} \\ -e^{2it} & 0 \end{pmatrix} + \sum_{i=1}^{N} T_i.$$

It follows that the exact formula for u and $|u|^2$ can be obtained as

$$u = \exp(2it) - 2\sum_{i=1}^{N} T_i[2,1],$$

$$|u|^2 = 1 + 2i\left(\sum_{i=1}^{N} T_i[1,1]\right)_x$$

$$= 1 - 2i\left(\sum_{i=1}^{N} T_i[2,2]\right)_x$$

$$= 1 + i\left(\sum_{i=1}^{N} T_i[1,1] - T_i[2,2]\right)_x,$$

where $T_i[m,n]$ represents the (m,n) element of matrix T_i. On the other hand, we have

$$\left(\frac{\Phi_i^{\dagger}\Phi_j}{\lambda_j - \bar{\lambda}_i}\right)_x = -i\Phi_i^{\dagger}\sigma_3\Phi_j.$$

Together with the above lemma, the exact rogue wave solution can be obtained by the limit technique [35,36]. ■

The formula $A_{l,j}$ can be rewritten as

$$A_{l,j} = \frac{i}{2}\sum_{m=0,\alpha\leqslant j-1\leqslant l+j+\alpha-m-2,}^{l+j-2}\ \sum_{\alpha=0,0\leqslant\alpha\leqslant m}^{j-1}\left(-\frac{1}{2}\right)^{l+j-m-2} \times C_{l+j-2-m}^{j-1-\alpha}(\psi_{m-\alpha}\bar{\psi}_{\alpha} + \phi_{m-\alpha}\bar{\phi}_{\alpha}), \tag{8}$$

where $C_m^n = \frac{m!}{n!(m-n)!}$. Indeed, we can prove the above equality by the following Taylor expansion:

$$\begin{aligned}
\frac{i(\psi\bar{\psi}+\phi\bar{\phi})}{2+f^2+\bar{f}^2} &= \frac{i}{2}\left[\sum_{i=0}^{\infty}\left(\sum_{j=0}^{i}(\psi_{i-j}\bar{\psi}_j + \phi_{i-j}\bar{\phi}_j)f^{2(i-j)}\bar{f}^{2j}\right)\right]\left[\sum_{j=0}^{+\infty}\left(-\frac{1}{2}\right)^j(f^2+\bar{f}^2)^j\right] \\
&= \frac{i}{2}\sum_{i=0}^{+\infty}\sum_{m=0}^{i}\left(-\frac{1}{2}\right)^{i-m}(f^2+\bar{f}^2)^{i-m}\left(\sum_{j=0}^{m}(\psi_{m-j}\bar{\psi}_j + \phi_{m-j}\bar{\phi}_j)f^{2(m-j)}\bar{f}^{2j}\right) \\
&= \frac{i}{2}\sum_{i=0}^{+\infty}\sum_{m=0}^{i}\left[\left(\sum_{j=0}^{m}(\psi_{m-j}\bar{\psi}_j + \phi_{m-j}\bar{\phi}_j)f^{2(m-j)}\bar{f}^{2j}\right)\left(-\frac{1}{2}\right)^{i-m}\sum_{\alpha=0}^{i-m}C_{i-m}^{\alpha}f^{2(i-m-\alpha)}\bar{f}^{2\alpha}\right] \\
&= \frac{i}{2}\sum_{i=0}^{+\infty}\sum_{m=0}^{i}\left[\left(-\frac{1}{2}\right)^{i-m}\sum_{l=0,j\leqslant l\leqslant i-m+j,}^{i}\ \sum_{j=0,0\leqslant j\leqslant m}^{l}C_{i-m}^{l-j}(\psi_{m-j}\bar{\psi}_j + \phi_{m-j}\bar{\phi}_j)f^{2(i-l)}\bar{f}^{2l}\right] \\
&= \frac{i}{2}\sum_{i=0}^{+\infty}\sum_{l=0}^{i}\left[\sum_{m=0,j\leqslant l\leqslant i-m+j,}^{i}\ \sum_{j=0,0\leqslant j\leqslant m}^{l}\left(-\frac{1}{2}\right)^{i-m}C_{i-m}^{l-j}(\psi_{m-j}\bar{\psi}_j + \phi_{m-j}\bar{\phi}_j)\right]f^{2(i-l)}\bar{f}^{2l}.
\end{aligned}$$

A transformation $i-l \to l-1, l \to j-1$ could obtain the formula (8).

III. THE APPLICATION OF THEOREM 1 AND THE TRAJECTORIES OF ROGUE WAVES

In order to illustrate how to use the above theorem, we give the following examples. Taking parameters $s_1 = a+ib$, $s_2 = c+id$, $s_j = 0$, $j \geqslant 3$, we have the following explicit expression:

$$\begin{aligned}
\psi_0 &= 2ix - 4t - i, \\
\psi_1 &= \left[\frac{2}{3}ix^3 - (4t+i)x^2 + \left(-8it^2 + 4t + \frac{1}{2}i\right)x + \frac{16}{3}t^3 + 4it^2 - 5t + \frac{1}{4}i - 2b + 2ia\right], \\
\psi_2 &= \left[\frac{1}{15}ix^5 - \left(\frac{2}{3}t + \frac{1}{6}i\right)x^4 + \left(-\frac{8}{3}it^2 + \frac{4}{3}t + \frac{1}{2}i\right)x^3 + \left(+\frac{16}{3}t^3 + 4it^2 - 7t - \frac{1}{4}i + 2ia - 2b\right)x^2\right. \\
&\quad + \left(\frac{16}{3}it^4 - \frac{16}{3}t^3 - 22it^2 + (5 - 8ib - 8a)t - \frac{1}{16}i + 2b - 2ia\right)x - \frac{32}{15}t^5 - \frac{8}{3}it^4 + 20t^3 \\
&\quad \left. + (-8ia + 8b + 9i)t^2 + \left(4a + 4ib - \frac{7}{8}\right)t - 2d + 2ic - \frac{1}{2}b + \frac{1}{2}ia - \frac{3}{32}i\right],
\end{aligned}$$

and

$$\phi_0 = 2x + 4it + 1,$$
$$\phi_1 = \left[\frac{2}{3}x^3 + (4it+1)x^2 + \left(-8t^2 + 4it + \frac{1}{2}\right)x - \frac{16}{3}it^3 - 4t^2 + 5it - \frac{1}{4} + 2ib + 2a\right],$$
$$\phi_2 = \left[\frac{1}{15}x^5 + \left(\frac{2}{3}it + \frac{1}{6}\right)x^4 + \left(-\frac{8}{3}t^2 + \frac{4}{3}it + \frac{1}{2}\right)x^3 + \left(-\frac{16}{3}it^3 - 4t^2 + 7it + 2a + 2ib + \frac{1}{4}\right)x^2 \right.$$
$$+ \left(\frac{16}{3}t^4 - \frac{16}{3}it^3 - 22t^2 + (5i - 8b + 8ia)t + 2a + 2ib - \frac{1}{16}\right)x + \frac{32}{15}it^5 + \frac{8}{3}t^4 - 20it^3$$
$$\left. + (-9 - 8ib - 8a)t^2 + \left(4ia + \frac{7}{8}i - 4b\right)t + 2c + \frac{1}{2}a + 2id + \frac{1}{2}ib + \frac{3}{32}\right].$$

Together with the formula (8), we have the following explicit expression $A_{l,j}$:

$$A_{11} = \frac{i}{2}(\psi_0\bar{\psi}_0 + \phi_0\bar{\phi}_0) = i\left(1 + 4x^2 + 16t^2\right),$$
$$A_{12} = \frac{i}{2}\left[-\frac{1}{2}(\psi_0\bar{\psi}_0 + \phi_0\bar{\phi}_0) + (\psi_1\bar{\psi}_0 + \phi_1\bar{\phi}_0)\right]$$
$$= \frac{1}{2}\left((16t + 8ix)a + (16it - 8x)b + \frac{8}{3}ix^4 - \frac{32}{3}x^3t + \left(-\frac{128}{3}t^3 - 24t\right)x - \frac{3}{2}i + 16it^2 - \frac{128}{3}it^4\right),$$
$$A_{21} = \frac{i}{2}\left[-\frac{1}{2}(\psi_0\bar{\psi}_0 + \phi_0\bar{\phi}_0) + (\psi_0\bar{\psi}_1 + \phi_0\bar{\phi}_1)\right]$$
$$= \frac{1}{2}\left((-16t + 8ix)a + (8x + 16it)b + \frac{8}{3}ix^4 + \frac{32}{3}x^3t + \left(\frac{128}{3}t^3 + 24t\right)x - \frac{3}{2}i + 16it^2 - \frac{128}{3}it^4\right),$$
$$A_{22} = \frac{i}{2}\left[\frac{1}{4}C_2^1(\psi_0\bar{\psi}_0 + \phi_0\bar{\phi}_0) - \frac{1}{2}\left[C_1^1(\psi_0\bar{\psi}_1 + \phi_0\bar{\phi}_1) + C_1^0(\psi_1\bar{\psi}_0 + \phi_1\bar{\phi}_0)\right] + (\psi_1\bar{\psi}_1 + \phi_1\bar{\phi}_1)\right]$$
$$= \frac{1}{4}\left[16ia^2 + \left(\frac{32}{3}ix^3 + (-128it^2 - 8i)x\right)a + 16ib^2 + \left(-\frac{256}{3}it^3 + 64ix^2t + 48it\right)b\right.$$
$$\left. + \frac{16}{9}ix^6 + \left(\frac{4}{3}i + \frac{64}{3}it^2\right)x^4 + \left(\frac{256}{3}it^4 + 160it^2 - i\right)x^2 + \frac{13}{4}i + 76it^2 - 64it^4 + \frac{1024}{9}it^6\right].$$

Furthermore, by formula (4) we can obtain that

$$|u[1]|^2 = 1 + [\ln(A_{11})]_{xx} = 1 + [\ln(1 + 4x^2 + 16t^2)]_{xx},$$
$$|u[2]|^2 = 1 + \left[\ln\begin{vmatrix} A_{11} & A_{12} \\ A_{21} & A_{22}\end{vmatrix}\right]_{xx} = 1 + [\ln(D_2)]_{xx},$$

where

$$D_2 = 144a^2 + (144x - 192x^3 + 2304xt^2)a + 144b^2 + (-1152x^2t + 864t + 1536t^3)b + 9 + 108x^2 + 1584t^2$$
$$+ 48x^4 + 6912t^4 + 768x^4t^2 + 64x^6 - 1152x^2t^2 + 4096t^6 + 3072x^2t^4. \quad (9)$$

Similar as above, we can obtain that

$$|u[3]|^2 = 1 + \left[\ln\left(\sum_{j=0}^{12} F_j x^j\right)\right]_{xx}.$$

The explicit expression of F_j is given in the Appendix.

We illustrate a simple formula of general rogue wave solution for NLS equation (1). Reference [49] was the original work giving the first five orders of rogue waves; a modified Darboux transformation was used. Many different methods have been performed to derive an Nth-order RW solution, such as the Hirota bilinear method [43], reduction method [44], algebraic geometry solution reduction method [45,46], and the generalized Darboux transformation method [35,37]. However, the formulas presented in these papers are all the ratio of two $2N \times 2N$ determinants. In this paper, we develop the generalized Darboux transformation method [35] to present a much simpler representation for Nth-order RWs with the ratio of $(N+1) \times (N+1)$-order determinant and $N \times N$-order determinant. The N-order and $2N$-order determinants have $N!$ terms and $(2N)!$ terms, respectively. As N is big enough, the terms of the $2N$-order determinant are much more than N order. Such as $N = 10$, we have $10! = 3\,628\,800$, $11! = 39\,916\,800$, $20! = 2\,432\,902\,008\,176\,640\,000$. Thus our formula simplifies the calculation tremendously. In addition,

by the formula (4), we can see the conservation law

$$\int_{-\infty}^{+\infty}(|u|^2-1)dx=\frac{[\det(A)]_x}{\det(A)}\Bigg|_{x=-\infty}^{x=+\infty}=0,$$

since $\det(A)$ is a polynomial of x.

The fundamental RW solution has been given for a long time [21], and its explicit formation can be given directly from the generalized expression (3) with $N=1$ as

$$\begin{aligned}u[1]&=\left(1-\frac{2}{A_{11}}\begin{vmatrix}A_{11}&\bar{\psi}_0\\ \phi_0&0\end{vmatrix}\right)\\&=\left(-1+\frac{4(1+4it)}{1+4x^2+16t^2}\right)e^{2it}.\end{aligned}\tag{10}$$

The solution corresponds to the well-known "eye" -shaped RW. Near $t=0$, the wave has the highest hump and there are two valleys around the hump [see Fig. 1(a)]. Long before or after $t=0$, the peak values of the hump and valley are close to the background. But the wave keeps the structure before or after the moment $t=0$. Therefore, we can define the trajectory by the motion of its hump and the valleys, which can be described by the motion of the hump and valleys' center locations [50]. The motion of its hump's center is calculated as

$$X_h=0,\tag{11}$$

and the motions of the two valleys' center are

$$X_v=\pm\sqrt{3}\left(t^2+\frac{3}{48}\right)^{1/2}.\tag{12}$$

Then, we can plot the RW's trajectory in Fig. 1(b). The trajectories of the two valleys look like an "X" shape, as shown by the red dashed lines in Fig. 1(b). The trajectory of the RW's hump is a straight line which traverses the center of the "X." Moreover, the straight line is one of the symmetric axes of the "X."

Furthermore, we can define the width of the RW as the distance between the two valleys' centers, which corresponds to the distance between the two red lines in Fig. 1(b). Its evolution is

$$W=2\sqrt{3}\left(t^2+\frac{3}{48}\right)^{1/2}.\tag{13}$$

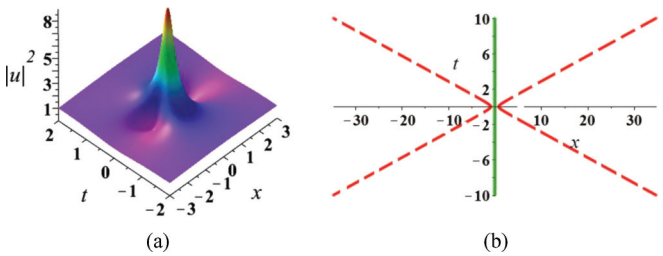

FIG. 1. (Color online) (a) The density evolution of the first-order RW. (b) The trace of the first-order RW. The green solid line corresponds to the trajectory of the RW's hump and the red dashed lines correspond to the trajectories of the RW's valleys. This holds for all pictures in the paper.

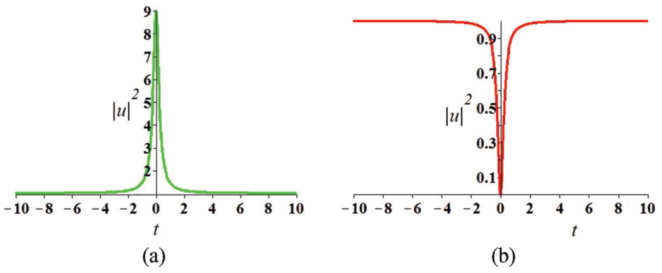

FIG. 2. (Color online) (a) The value evolution of the RW's hump. (b) The value evolution of the RW's valleys.

Obviously, the width is compressed before the moment $t=0$ when the highest peak emerges and is broadened after the moment.

Inserting (11) and (12) into the density expression of (10), one can obtain explicit expressions for the evolution of the RW's hump and valleys, shown in Fig. 2. It is seen that the highest value of the RW is nine times the value of background [49]. Comparing Figs. 1(b) and 2, we know that the RW has the highest and steepest structure when the width is the smallest. Namely, the width is broadened or compressed with time, and the peak decreases or increases correspondingly from the modulation instability effect.

A higher-order RW solution has been presented in [35,43,49]. It is known that the second-order rogue wave possesses different dynamics. Choosing the parameter $s_1=a+ib$, we can readily obtain the general second-order rogue wave solution by formula (3):

$$\begin{aligned}u[2]&=\left(1-\frac{2}{\begin{vmatrix}A_{11}&A_{12}\\A_{21}&A_{22}\end{vmatrix}}\begin{vmatrix}A_{11}&A_{12}&\bar{\psi}_0\\A_{21}&A_{22}&\bar{\psi}_1\\ \phi_0&\phi_1&0\end{vmatrix}\right)\\&=\left(1+\frac{D_1}{D_2}\right)e^{2it},\end{aligned}$$

$$\begin{aligned}D_1=&(-576x-2304ixt)a+(144i-2304it^2-1152t\\&+576ix^2)b-768ix^4t-192x^4-1536it^3-288x^2\\&-3456t^2+36-4608x^2t^2-12288it^5+720it\\&-6144it^3x^2+1152ix^2t-15360t^4,\end{aligned}$$

D_2 is given in Eq. (9).

The trajectory of the first-order rogue wave can be derived exactly. However, for the second-order rogue wave, we cannot obtain an exact expression for the trajectory of the second-order rogue wave, since the high-order algebraic equation emerges for these extreme points. When x or $t\to\infty$, we can readily prove that the trajectory of the second-order rogue wave is asymptotic to the first-order rogue wave. But we cannot obtain the trajectory of the second-order rogue wave in the neighbourhood of $(x,t)=(0,0)$ in a simple way. To give the trajectory of the second-order rogue wave, we use the numerical method. We know that the locations of humps and valleys can be used to describe the RW's trajectory. Thus we just need to obtain the trajectories of these extreme points.

We merely consider the three special cases for the second-order rogue wave solution. First, we give the trace for the standard second-order rogue wave solution in Figs. 3(a) and 3(b), which is symmetrical about both the x and t axes.

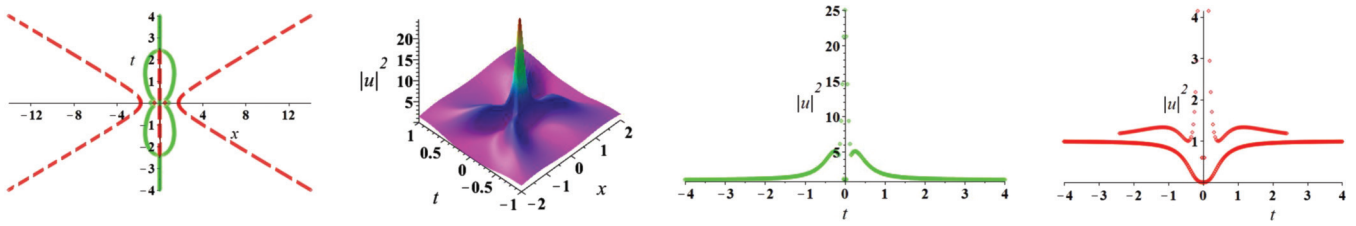

(a) (b) (c) (d)

FIG. 3. (Color online) Standard second-order RW: (a) The trajectory of the second-order RW which is symmetrical about the x and t axis. (b) The density evolution of the second-order RW. (c) The value evolution of the RW's hump peak. (d) The value evolution of the RW's valleys. The parameters are $a = 0$ and $b = 0$.

We use the numerical method to derive the peak value curve and hole value curve for the standard second-order rogue wave [Figs. 3(c) and 3(d)]. Comparing the trajectory in Fig. 3 with that in Fig. 1, we know that the whole trajectories of them are similar, but the trajectories and structures are distinctive from each other near the location where the highest peak emerges. Comparing the curves in Figs. 3(c) and 3(d) with Fig. 2, we can see that the two curves are very similar. But they possess different peak values. The maximum of the peak value curve for the second-order rogue wave is 25. But the maximum of the hump value curve for the first-order rogue wave is 9. The valley value of the second-order rogue wave is also similar to the first-order rogue wave. But the valley curve near $t = 0$ is higher than the background, and the maximum of the curve is about 4.2.

For the second-order RW, there can be three symmetry RWs in the temporal-spatial distribution [51]. As examples, we give two other special cases for the trajectory of the second-order rogue wave solution in Fig. 4, which are symmetrical about the x and t axes separately. From the pictures, we can see that the trajectory of the RW is consistent with the fundamental RW. Each center of the "X" shape corresponds to the highest peak's location. This can be verified by comparing the locations in Fig. 4.

IV. THE CLASSIFICATION OF HIGH-ORDER ROGUE WAVES BY PARAMETERS

In this section, we give the classification of high-order rogue waves through parameter s_i. For instance, there is no parameter s_i in the standard first-order RW. So there is only one kind. The general second-order RW has one parameter s_1; we classify it by whether or not the parameter s_1 equals zero. If parameter $s_1 = 0$, we denote it as type [0]. Otherwise, we denote it as type [1]. The general third-order RW has two parameters, s_1 and s_2 (Fig. 5). We still classify it by whether or not the parameters s_1,s_2 equal zero. If $s_1 = s_2 = 0$, this is the standard case; we denote it as type [0,0]. The other cases are types [0,1], [1,0], and [1,1]. Similarly, the general fourth-order RW has three parameters, s_1, s_2, and s_3. Then the types are [0,0,0], [1,0,0], [0,1,0], [0,0,1], [1,1,0], [1,0,1], [0,1,1], and [1,1,1].

Indeed, there are lots of interesting spatial-temporal distribution pictures hiding in our classification. For instance, in the general second-order RW, type [0] corresponds to the standard one and type [1] corresponds to the "triplets" [51]. For the general third-order rogue wave, type [0,0] corresponds to the "standard" structure [49], type [1,0] corresponds to the "triangular cascade" structure [42], and type [0,1] corresponds to the "pentagram" structure [42]. The "claw" structure [41] and the "arrow" structure [41] are all involved in type [1,1]. The claw structure was first derived in Ref. [41] by numeric method. Different from them, we also present the claw structure of the third-order RW by explicit analytical expression with proper ratio to parameters s_1 and s_2 [Fig. 6(a)]. But we fail to find the explicit ratio value and just report its existence.

The general fourth-order RW is obtained by formula (3). From previous research [35], we know that type [0,0,0] corresponds to the standard structure [49], type [1,0,0] corresponds to the "triangle" structure [42], type [0,1,0] corresponds to the pentagram structure [42], and type [0,0,1] corresponds to the "heptagram" structure [42]. In the following, we look

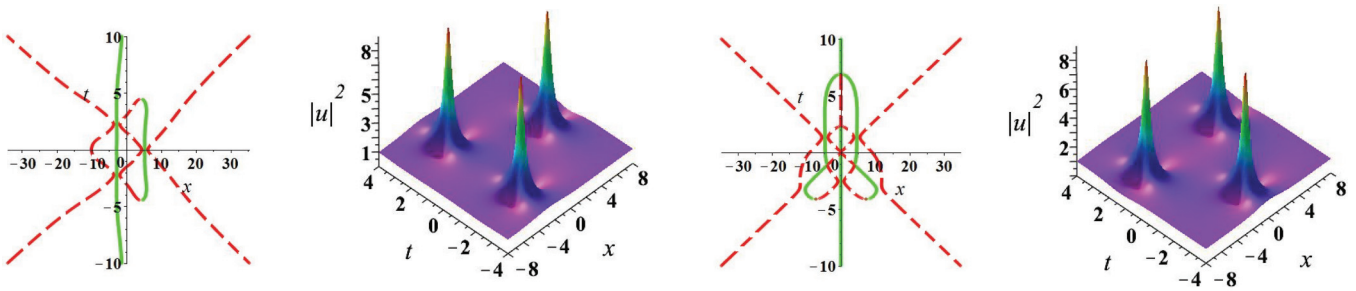

(a) (b) (c) (d)

FIG. 4. (Color online) (a) The trajectory of the second-order RW which is symmetrical about the x axis with parameters $a = 100$ and $b = 0$. (b) The density evolution of the second-order RW in (a). (c) The trajectory of the second-order RW which is symmetrical about the t axis with parameters $a = 0$ and $b = 100$. (d) The density evolution of the second-order RW in (c).

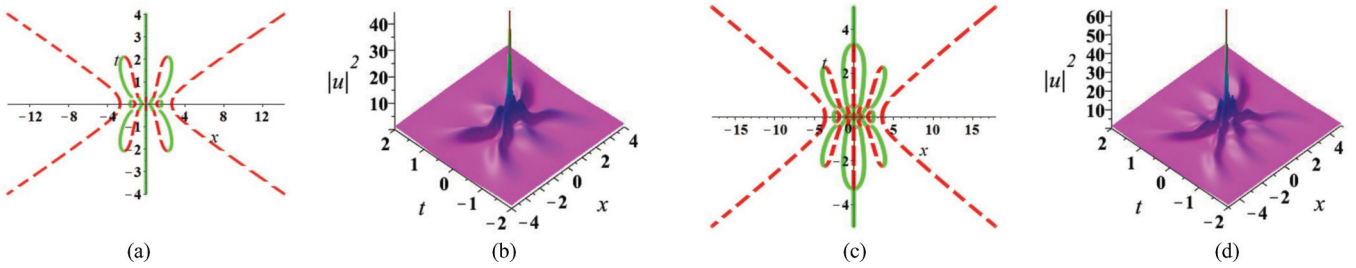

FIG. 5. (Color online) (a) The trajectory of the third-order RW which is symmetrical about the x and t axes. (b) The density evolution of the third-order RW. (c) The trajectory of the fourth-order RW which is symmetrical about the x and t axes. (d) The density evolution of the fourth-order RW.

for some interesting structures in the other four types. First, we look for an interesting structure in type [1,1,1]. Choosing the parameters s_1, s_2, and s_3 with proper proportion, we can obtain the standard claw-like RW [Fig. 6(b)], which possesses one third-order RW and four first-order RW structures. This structure has been obtained in Ref. [41] by numeric method. Here we also obtain it by the explicit rational expression. Secondly, we search the interesting structures in type [1,0,1]. By choosing the parameters s_1 and s_3 with proper ratio and $s_2 = 0$, we can obtain a different kind of structure, the "double column" structure [Fig. 7(a)], which possesses two standard second-order RWs and four first-order RWs. Finally, we obtain two other types of clawlike RW structures in type [0,1,1] and [1,1,0], respectively. The first type, the "claw-line-I" structure type, is shown in Fig. 7(b). This type of RW can be obtained by setting parameters s_2 and s_3 with appropriate ratio and $s_1 = 0$. This RW possesses a standard second-order RW and seven first-order RWs, for which the four fundamental RWs arrange in an arc, and the other three fundamental RWs arrange in a line. The second type, the "claw-line-II" RW is shown in Fig. 8(a), which possesses a similar structure with one second-order RWs and seven first-order RWs, which can be obtained by choosing s_1 and s_2 with proper ratio and $s_3 = 0$. Among them, the five fundamental RWs arrange in an arc; the other two fundamental RWs are located in the outer edge of the arc. Indeed, there may exist other interesting temporal-spatial distribution pictures [52]. Here we merely list some interesting structures.

For general high-order rogue wave solution, we have the following classification. The general Nth-order rogue wave solution possesses $N-1$ parameters. So it possesses 2^{N-1} cases. As the order increases, the types of structures become more and more abundant. In this paper, we do not research it in detail. As an example, we show the sixth-order RW with "circle-arc" structure [Fig 8(b)], which consists of an "enneagram" with a circle boundary and an "arc" with six fundamental RWs arranged. This is a different structure for sixth-order RWs, which would enrich our knowledge about complex localized waves in the related physical systems.

V. DISCUSSION AND CONCLUSION

We propose a simple representation for generalized RW solution, which can be used to obtain an arbitrary order RW solution and observe its dynamics conveniently. Based on the solution, we investigate the trajectories of them through defining the properties function. We find that the fundamental RW's valleys have "X" -shaped trajectories. For higher-order RWs, the whole trajectory is similar to that of the fundamental one. But they are different near the moment when the highest peak emerges, such as the trajectories of the third-order and

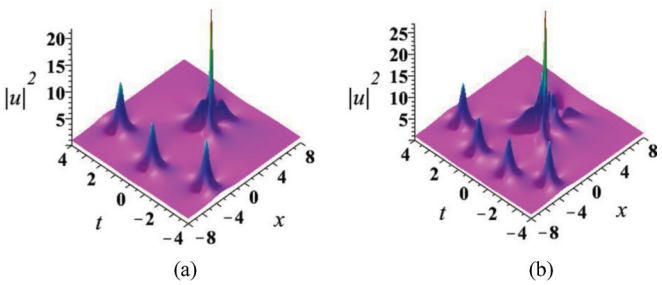

FIG. 6. (Color online) (a) The "clawlike" structure of the third-order rogue wave with $s_1 = 31.2$, $s_2 = 500$. On the left side, there are three RWs that form an arc. On the right side, there is a second-order RW with the highest peak. (b) The standard claw structure of the fourth-order RW with $s_1 = 12$, $s_2 = 101.025$, and $s_3 = 1016$. On the left side, there are four RWs forming an arc. On the right side, there is a third-order RW with the highest peak.

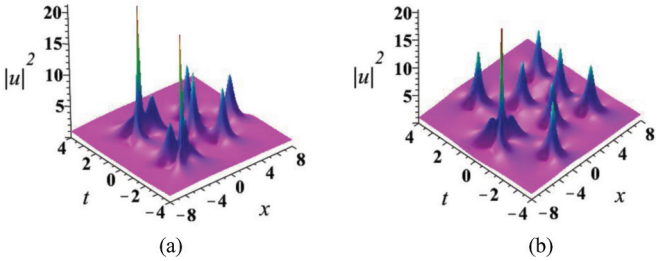

FIG. 7. (Color online) (a) The double column structure of the fourth-order rogue wave with $s_1 = 9$, $s_2 = 0$, $s_3 = 453$. There are two second-order RWs on the left side, which look like two columns. On the right side, there are four first-order RWs arranging in a quadrangle. (b) The claw-line-I structure of the fourth-order RW with $s_2 = 104$, $s_3 = 940$, $s_1 = 0$. On the left side, there is a clawlike structure. And the number of claw is 4. Besides this, there are three RWs arranged in a line. Thus we call it "claw-line-I" type.

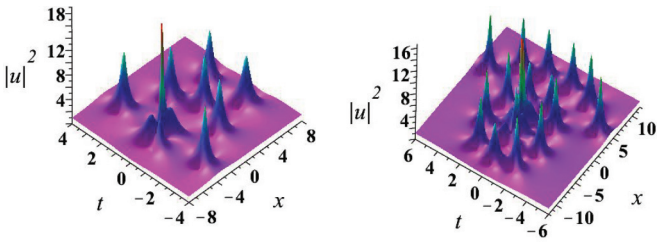

FIG. 8. (Color online) (a) The claw-line-II structure of the fourth-order RW with $s_1 = 8$, $s_2 = 108$, $s_3 = 0$. On the leftside, there is a clawlike structure. And the number of claw is 5. In addition, there are two RWs arranged in a line on the right side. Thus we call it "claw-line-II" type. (b) The circle-arc structure of the sixth-order RW with $s_1 = -12$, $s_2 = -100$, $s_3 = -1000$, $s_4 = -10800$, $s_5 = -150000$. There is a enneagram on the left side. The remaining six fundamental RWs arrange in an arc.

fourth-order RWs in Fig. 5. Finally, the classification of the general high-order RW solution is discussed. We find some different structures for high-order RWs by choosing different parameters with some proper ratios, such as the double column structure, claw-line structure, and circle-arc structure. But we fail to obtain the exact value of the ratio for these different RW structures. The systemic classification on them should be done in the near future.

ACKNOWLEDGMENTS

The authors thank the anonymous referees for their valuable suggestions. This work is supported by the National Fundamental Research Program of China (Contract No. 2011CB921503) and the National Science Foundation of China (Contracts No. 11274051, No. 91021021, and No. 11271052).

APPENDIX: THE EXPLICIT EXPRESSIONS OF F_j

$$
\begin{aligned}
F_0 &= 36 + 4608ac + 18\,432a^2b^2 + 2304d^2 + 2304c^2 + 9216a^4 + 9216b^4 + 3456b^2 + 3456a^2 + 4608bd \\
&\quad + (18\,432b + 36\,864a^2d - 36\,864b^2d + 11\,520\,d - 73\,728abc + 73\,728a^2b + 73\,728b^3)t \\
&\quad + (129\,024a^2 + 26\,496 + 36\,864c^2 + 276\,480b^2 + 36\,864d^2 - 110\,592ac - 110\,592bd)t^2 \\
&\quad + (-98\,304b^3 - 98\,304a^2b - 36\,864d + 620\,544b)t^3 + (196\,608ac + 49\,152a^2 - 540\,672b^2 + 196\,608bd + 654\,336)t^4 \\
&\quad + \left(\frac{3\,342\,336}{5}d - \frac{2\,064\,384}{5}b\right)t^5 + \left(\frac{1\,835\,008}{5}a^2 + \frac{786\,432}{5}b^2 + 11\,14\,112\right)t^6 \\
&\quad + \left(\frac{8\,912\,896}{5}b + \frac{1\,048\,576}{5}d\right)t^7 + \frac{21\,757\,952}{5}t^8 + \frac{8\,388\,608}{15}bt^9 + \frac{58\,720\,256}{25}t^{10} + \frac{67\,108\,864}{225}t^{12}, \\
F_1 &= 18\,432b^2c - 36\,864abd + 2304a - 18\,432a^2c + 1152c + (110\,592bc - 110\,592ad)\,t \\
&\quad + (-147\,456ab^2 - 147\,456a^3 + 202\,752c + 82\,944a)t^2 + (-196\,608ad + 196\,608bc - 983\,040ab)t^3 \\
&\quad + (884\,736c - 737\,280a)\,t^4 - \frac{3\,145\,728}{5}abt^5 + \left(524\,288c - \frac{262\,144}{5}a\right)t^6 + \frac{4\,194\,304}{5}at^8, \\
F_2 &= -9216ac + 864 + 9216c^2 + 9216d^2 - 9216bd - 4608a^2 - 4608b^2 + (-41\,472b + 73\,728b^3 - 46\,080d + 73\,728a^2b)t \\
&\quad + (663\,552b^2 + 73\,728a^2 - 41\,472)t^2 + (-294\,912d + 1\,622\,016b)\,t^3 + (1\,425\,408 + 589\,824b^2 - 196\,608a^2)t^4 \\
&\quad + \left(\frac{12\,976\,128}{5}b - \frac{2\,359\,296}{5}d\right)t^5 + 3\,932\,160t^6 + \frac{6\,291\,456}{5}t^8 + \frac{33\,554\,432}{75}t^{10}, \\
F_3 &= -4608c + 12\,288a^3 - 3840a + 12\,288ab^2 + (49\,152bc + 147\,456ab - 49\,152ad)\,t \\
&\quad + (270\,336a + 49\,152c)\,t^2 + 524\,288abt^3 + (-131\,072c + 1\,638\,400a)\,t^4 + \frac{8\,388\,608}{15}at^6, \\
F_4 &= 3072b^2 + 15\,360a^2 - 12\,288\,ac - 12\,288bd + 960 + (18\,432b - 36\,864d)\,t + (147\,456a^2 - 49\,152b^2 + 61\,440)t^2 \\
&\quad + (-65\,536\,d - 294\,912\,b)\,t^3 - 98\,304t^4 - \frac{1\,048\,576}{5}bt^5 + \frac{1\,048\,576}{15}t^6 + \frac{4\,194\,304}{15}\,t^8, \\
F_5 &= -\frac{18\,432}{5}c + \frac{27\,648}{5}a - \frac{196\,608}{5}bat + \left(-\frac{294\,912}{5}c - \frac{49\,152}{5}a\right)t^2 + \frac{524\,288}{5}at^4, \\
F_6 &= \frac{12\,288}{5}a^2 + \frac{13\,312}{5} + \frac{28\,672}{5}b^2 + \left(16\,384d + \frac{8192}{5}b\right)t + \frac{49\,152}{5}t^2 - \frac{1\,048\,576}{15}bt^3 - \frac{262\,144}{5}t^4 + \frac{4\,194\,304}{45}t^6, \\
F_7 &= \frac{8192}{5}c - \frac{4096}{5}a, \quad F_8 = \frac{3072}{5} - \frac{32\,768}{5}bt - \frac{32\,768}{5}t^2 + \frac{262\,144}{15}t^4, \\
F_9 &= -\frac{16\,384}{15}a, \quad F_{10} = \frac{8192}{75} + \frac{131\,072}{75}t^2, \quad F_{11} = 0, \quad F_{12} = \frac{16\,384}{225}.
\end{aligned}
$$

[1] V. Ruban, Y. Kodama, M. Ruderman, J. Dudley, R. Grimshaw, P. V. E. McClintock, M. Onorato, C. Kharif, E. Pelinovsky, T. Soomere, G. Lindgren, N. Akhmediev, A. Slunyaev, D. Solli, C. Ropers, B. Jalali, F. Dias, and A. Osborne, Eur. Phys. J.: Spec. Top. **185**, 5 (2010).

[2] N. Akhmediev and E. Pelinovsky, Eur. Phys. J.: Spec. Top. **85**, 1 (2010).

[3] C. Kharif and E. Pelinovsky, Eur. J. Mech. B/Fluids **22**, 603 (2003).

[4] A. R. Osborne, *Nonlinear Ocean Waves* (Academic Press, New York, 2009).

[5] E. Pelinovsky and C. Kharif, *Extreme Ocean Waves* (Springer, Berlin, 2008).

[6] B. Kibler, J. Fatome, C. Finot, G. Millot, F. Dias, G. Genty, N. Akhmediev, and J. M. Dudley, Nat. Phys. **6**, 790 (2010).

[7] A. Chabchoub, N. P. Hoffmann, and N. Akhmediev, Phys. Rev. Lett. **06**, 204502 (2011).

[8] H. Bailung, S. K. Sharma, and Y. Nakamura, Phys. Rev. Lett. **107**, 255005 (2011).

[9] A. R. Osborne, Mar. Struct. **4**, 275 (2001); N. Akhmediev, A. Ankiewicz, and M. Taki, Phys. Lett. A **373**, 675 (2009).

[10] Yu. V. Bludov, V. V. Konotop, and N. Akhmediev, Phys. Rev. A **80**, 033610 (2009).

[11] A. Newell and J. Moloney, *Nonlinear Optics* (Addison-Wesley, Redwood City, CA, 1992).

[12] C. Kharif, E. Pelinovsky, and A. Slunyaev, *Rogue Waves in the Ocean* (Springer-Verlag, New York, 2009).

[13] C. Sulem and P. Sulem, *The Nonlinear Schrödinger Equation: Self-Focusing and Wave Collapse* (Springer, Berlin, 1999), Vol. 139.

[14] L. P. Pitaevskii and S. Stringari, *Bose-Einstein Condensation* (Oxford University Press, Oxford, UK, 2003), Vol. 116.

[15] Y. C. Ma, Stud. Appl. Math. **60**, 43 (1979).

[16] N. Akhmediev, V. M. Eleonskii, and N. Kulagin, Zh. Eksp. Teor. Fiz. **98**, 1542 (1985).

[17] N. Akhmediev and V. I. Korneev, Theor. Math. Phys. **69**, 1089 (1986).

[18] M. J. Lighthill, J. Inst. Math. Appl. **1**, 269 (1965).

[19] T. B. Benjamin and J. E. Feir, J. Fluid Mech. **27**, 417 (2006).

[20] H. C. Yuen and B. M. Lake, Adv. Appl. Mech. **22**, 67 (1982).

[21] D. H. Peregrine, J. Aust. Math. Soc. Ser. B, Appl. Math. **25**, 16 (2009).

[22] A. Chabchoub, N. P. Hoffmann, M. Onorato, and N. Akhmediev, Phys. Rev. X **2**, 011015 (2012).

[23] A. Chabchoub, N. Hoffmann, M. Onorato, A. Slunyaev, A. Sergeeva, E. Pelinovsky, and N. Akhmediev, Phys. Rev. E **86**, 056601 (2012).

[24] M. Onorato, D. Proment, G. Clauss, and M. Klein, PloS ONE **8**, e54629 (2013).

[25] M. Erkintalo, K. Hammani, B. Kibler, C. Finot, N. Akhmediev, J. M. Dudley, and G. Genty, Phys. Rev. Lett. **107**, 253901 (2011).

[26] P. Shukla and W. Moslem, Phys. Lett. A **376**, 1125 (2012).

[27] R. Sabry, W. M. Moslem, and P. K. Shukla, Phys. Rev. E **86**, 036408 (2012).

[28] V. B. Matveev and M. A. Salle, *Darboux Transformation and Solitons* (Springer-Verlag, Berlin, 1991).

[29] J. L. Cieslinski, J. Phys. A **42**, 404003 (2009).

[30] E. V. Doktorov and S. B. Leble, *A Dressing Method in Mathematical Physics* (Springer-Verlag, Berlin, 2007).

[31] M. Adler and J. Moser, Commun. Math. Phys. **61**, 1 (1978).

[32] G. Neugebauer and R. Meinel, Phys. Lett. A **100**, 467 (1984).

[33] Y. Li, X. Gu, and M. Zou, Acta Math. Sinica **3**, 143 (1987).

[34] C. L. Terng and K. Uhlenbeck, Commun. Pure Appl. Math. **53**, 1 (2000).

[35] B. Guo, L. Ling, and Q. P. Liu, Phys. Rev. E **85**, 026607 (2012).

[36] B. Guo, L. Ling, and Q. P. Liu, Stud. Appl. Math. **130**, 317 (2013).

[37] J. S. He, H. R. Zhang, L. H. Wang, K. Porsezian, and A. S. Fokas, Phys. Rev. E **87**, 052914 (2013).

[38] L. Li, Z. Wu, L. Wang, and J. He, Ann. Phys. **334**, 198 (2013).

[39] D. J. Kedziora, A. Ankiewicz, and N. Akhmediev, Phys. Rev. E **84**, 056611 (2011).

[40] D. J. Kedziora, A. Ankiewicz, and N. Akhmediev, Phys. Rev. E **86**, 056602 (2012).

[41] D. J. Kedziora, A. Ankiewicz, and N. Akhmediev, Phys. Rev. E **85**, 066601 (2012).

[42] D. J. Kedziora, A. Ankiewicz, and N. Akhmediev, Phys. Rev. E **88**, 013207 (2013).

[43] Y. Ohta and J. K. Yang, Proc. R. Soc. London, Ser. A **468**, 1716 (2012).

[44] P. Dubard, P. Gaillard, C. Klein, and V. B. Matveev, Eur. Phys. J.: Spec. Top. **185**, 247 (2010).

[45] P. Gaillard, J. Phys. A: Math. Theor. **44**, 435204 (2011).

[46] C. Kalla, J. Phys. A: Math. Theor. **44**, 335210 (2011).

[47] M. J. Ablowitz, D. J. Kaup, A. C. Newell, and H. Segur, Stud. Appl. Math. **53**, 249 (1974).

[48] V. E. Zakharov and S. V. Manakov, JETP Lett. **8**, 243 (1973).

[49] N. Akhmediev, A. Ankiewicz, and J. M. Soto-Crespo, Phys. Rev. E **80**, 026601 (2009).

[50] L. C. Zhao, Ann. Phys. **329**, 73 (2013).

[51] N. Akhmediev, A. Ankiewicz, J. M. Soto-Crespo, and J. M. Dudley, Phys. Lett. A **375**, 541 (2011).

[52] P. Gaillard, J. Math. Phys. **54**, 073519 (2013).